

New efficient optimal mass transport approach for single freeform surface design

Christoph Bösel^{1,*} and Herbert Gross¹

¹*Friedrich-Schiller-Universität Jena, Institute of Applied Physics,
Abbe Center of Photonics, 07743 Jena, Germany*

We present a new optimal mass transport approach for the design of a continuous single freeform surface for collimated beams. By applying the law of reflection/refraction and the well-known integrability condition, it is shown that the design process in a small angle approximation can be decoupled into the calculation of a raymapping by optimal mass transport methods and the subsequent construction of the freeform surface by a steady linear advection equation. It is shown that the solution of this linear advection equation can be obtained by a decomposition into two dimensional subproblems and solving these by standard integrals. The efficiency of the method is demonstrated by applying it to two challenging design examples.

PACS numbers: 42.15.-i, 42.15.Eq.

I. INTRODUCTION

In recent years much progress has been made in the field of freeform surface design without the assumption of symmetries [1–14]. The goal of these design methods is the solution of the so called inverse problem of nonimaging optics. This means that for given arbitrary source and target intensities $I_S(x, y)$ and $I_T(x, y)$ one or more freeform surfaces have to be calculated, which map the intensities onto each other.

The first successful method at calculating a continuous freeform surface utilizing a complex target intensity was developed by Ries and Muschaweck [1], but unfortunately the numerical method was not published [1]. Their approach is able to handle the far field design problem for single freeform surfaces illuminated by a point source [1]. Nowadays, many other methods have been developed by different research groups. A quite popular approach are the so-called Monge-Ampre methods [2–6]. They are based on the modelling of the design problem by a non-linear partial differential equation of Monge-Ampre type and solving it with sophisticated numerical techniques. These methods are able to handle the design problem in the far field for intensity control of point sources [2] and collimated beams [4, 6] as well as intensity and phase control with double freeform surfaces [5].

Another popular approach for the single freeform surface design with point sources is the supporting ellipsoids method developed by Oliker [7]. With this method a freeform mirror is constructed by putting a point source in the focal point of a unification of ellipsoids, whereby every ellipsoid has a different position of the second focal point on the target plane to build the required intensity pattern. The problem with this method is the calculation of a smooth freeform surface by the unification of the ellipsoids. Therefore it was further developed by other research groups [8, 9] and generalized to calculate freeform lenses [10]. It can handle the far field as well as the near

field design problem.

The approach we will concentrate on in this work are the optimal mass transport (OMT) methods, which gained some interest in recent years and are partly based on the mathematical concept of optimal mass transport as explained in the following paragraph. They can handle the design problem of a single freeform surface for intensity control [11, 12] as well as double freeform surfaces for intensity and phase control [11–14].

This approach for the freeform surface design consists of two separate steps. In the first step a ray mapping between the given input and output intensities is calculated via OMT. In the second step the freeform surface is constructed with the help of the law of refraction/reflection and an integrability condition, which ensures the continuity of the surface in a way that the input rays hit the target plane according to the optimal mapping.

The difference between the two OMT methods mentioned above is the second step. In first approach by Buerle *et al.* the freeform is constructed by an optimization procedure [11, 12], while the second approach by Feng *et al.* uses a simultaneous point-by-point construction method to design a double freeform surface [13, 14].

Since these attempts seem to be quite successful but do not give insights about the existence of a continuous solution to the freeform surface design problem for a given ray mapping, we want to clarify this point in our work for a single freeform illuminated by a collimated beam. Based on our findings, we developed a new effective numerical freeform surface construction approach. To do so this paper is structured as follows.

In section II after a short introduction to the OMT and a presentation of its basic properties, we will derive from the law of reflection/refraction and the integrability condition a partial differential equation for the direct calculation of a continuous freeform surface. It will be shown that for the optimal mapping and a small angle approximation the freeform surface design indeed decouples into the two step process described above. In section III we then show that the PDE for the lens construction can be solved by simple integrations. The efficiency of this approach is then shown in section IV by applying it to two

* christoph.boesel@uni-jena.de

challenging design examples, followed by a discussion of our results in section V.

II. DESIGN METHOD

A. Optimal mass transport

The problem statement of OMT, also called the Monge-Kantorovich problem, is as follows: two positive density functions $I_S(\mathbf{x})$ and $I_T(\mathbf{x})$ with

$$\int_{\mathbb{R}^N} I_S(\mathbf{x}) d\mathbf{x} = \int_{\mathbb{R}^N} I_T(\mathbf{x}) d\mathbf{x} \quad (1)$$

have to be mapped onto each other according to the Jacobi equation

$$\det(\nabla \mathbf{u}(\mathbf{x})) I_T(\mathbf{u}(\mathbf{x})) = I_S(\mathbf{x}) \quad (2)$$

with a smooth, bijective mapping $\mathbf{u}(\mathbf{x})$. If M is defined as the set of mappings fulfilling equation (2), we are searching for a mapping minimizing the transport cost according to the Kantorovich-Wasserstein distance

$$d(I_S, I_T)^N = \inf_{\mathbf{u} \in M} \int |\mathbf{u}(\mathbf{x}) - \mathbf{x}|^N I_S(\mathbf{x}) d\mathbf{x}, \quad (3)$$

whereby $\inf_{\mathbf{u} \in M}$ denotes the mapping for which the integral has its minimal value. These optimal mapping, which is defined by (1), (2) and (3), has the useful property that it is unique [15] and it is characterized by a vanishing curl [16]. The latter property will be important for our findings in the next subsection.

In the special case of freeform surface design considered here, the densities $I_S(\mathbf{x})$ and $I_T(\mathbf{x})$ correspond to the source and target intensities (see Fig. 1). Therefore equation (1) describes a global and equation (2) a local energy conservation.

For the numerical examples in section IV, we have implemented the OMT method developed by Sulman *et al.* [17]. It provides a good compromise between an easy implementation and an effective mapping calculation and is thus sufficient for our test purposes.

The result of this design process step is therefore the mapping $\mathbf{u}(x, y)$.

B. Freeform surface construction

1. Surface equation

In the following, we want to derive a differential equation for the direct calculation of a freeform surface for a given ray mapping $\mathbf{u}(x, y)$. To do so, two basic equations are considered. On the one hand, for an incoming beam described by the ray direction vector field \mathbf{s}_1 and the refracted vector field \mathbf{s}_2 , the law of refraction

$$\mathbf{n} = n_1 \hat{\mathbf{s}}_1 - n_2 \hat{\mathbf{s}}_2, \quad (4)$$

with the refractive indices n_1 of the lens and n_2 of the surrounding medium, has to be fulfilled. On the other hand, we want to ensure the continuity of the surface $z(x, y)$ by the well-known integrability condition [1]

$$\mathbf{n} \cdot (\nabla \times \mathbf{n}) = 0. \quad (5)$$

Since the collimated beam \mathbf{s}_1 as well as \mathbf{s}_2 can be expressed in terms of the unknown freeform surface $z(x, y)$ and the given ray mapping $\mathbf{u}(x, y)$ (see Fig. 1):

$$\mathbf{s}_1 = \begin{pmatrix} 0 \\ 0 \\ z(x, y) \end{pmatrix}, \quad \mathbf{s}_3 = \begin{pmatrix} u_x(x, y) - x \\ u_y(x, y) - y \\ z_T \end{pmatrix}, \quad \mathbf{s}_2 = \mathbf{s}_3 - \mathbf{s}_1, \quad (6)$$

the equations (4) and (5) represent a differential equation for $z(x, y)$. Plugging (4) into equation (5) the integrability condition can be written in the form (see Appendix A)

$$\mathbf{s}_2(\nabla \times \mathbf{s}_1) = n_1 \frac{\{\mathbf{s}_2 \times [(\mathbf{s}_2 \nabla) \mathbf{s}_2]\}_z}{\mathbf{n} \cdot \mathbf{s}_2} + \mathbf{s}_2(\nabla \times \mathbf{s}_3), \quad (7)$$

which holds for a *general* ray mapping $\mathbf{u}(x, y)$. Equation (7) is organized in a way that only the left-hand side (LHS) depends on the derivatives of $z(x, y)$. Equation (7) takes a more familiar form by inserting the vector fields (6), which leads to

$$\mathbf{v} \nabla z(x, y) = n_1 \cdot \frac{\mathbf{v} \cdot [(\mathbf{v}^\perp \cdot \nabla) \mathbf{v}^\perp]}{\mathbf{n} \cdot \mathbf{s}_2} - (z_T - z(x, y)) \nabla \mathbf{v}, \quad (8)$$

with the velocity field $\mathbf{v} = (\mathbf{u}(x, y) - \mathbf{Id})^\perp$, the identity vector $\mathbf{Id} = (x, y)^T$ and $\nabla^\perp = (-\partial_y, \partial_x)$. This equation is a semilinear two dimensional advection equation, whereby the unknown surface $z(x, y)$ corresponds to conserved transport quantity and the right-hand side (RHS) to a source term.

In principle one could try to solve equation (8) after applying suitable boundary conditions, but as it will be demonstrated, it is not appropriate for finding a continuous freeform surface. This can be seen easily by considering the condition that the normalized vector field (4) has to be equal to the gradient of the surface $z(x, y)$:

$$\nabla(z - z(x, y)) \stackrel{!}{=} \frac{\mathbf{n}}{(\mathbf{n})_z} \Leftrightarrow \begin{pmatrix} -\partial_x z(x, y) \\ -\partial_y z(x, y) \\ 1 \end{pmatrix} \stackrel{!}{=} \begin{pmatrix} -\frac{n_2}{|\mathbf{s}_2| \cdot (\mathbf{n})_z} v_y \\ \frac{n_2}{|\mathbf{s}_2| \cdot (\mathbf{n})_z} v_x \\ 1 \end{pmatrix}. \quad (9)$$

Plugging this relation into the LHS of (8), we get $\mathbf{v} \nabla z(x, y) \equiv 0$, which can only be fulfilled if the RHS vanishes:

$$n_1 \cdot \frac{\mathbf{v} \cdot [(\mathbf{v}^\perp \cdot \nabla) \mathbf{v}^\perp]}{\mathbf{n} \cdot \mathbf{s}_2} - (z_T - z(x, y)) \nabla \mathbf{v} \stackrel{!}{=} 0. \quad (10)$$

Since $\mathbf{v} \perp (\mathbf{u}(x, y) - \mathbf{Id})$ and therefore $(\mathbf{u}(x, y) - \mathbf{Id}) \parallel \nabla z(x, y)$ the necessity of the vanishing source term reflects the nature of the law of refraction, that the vectors $\mathbf{s}_1(x, y)$, $\mathbf{s}_2(x, y)$ and $\mathbf{n}(x, y)$ have to lie in the same

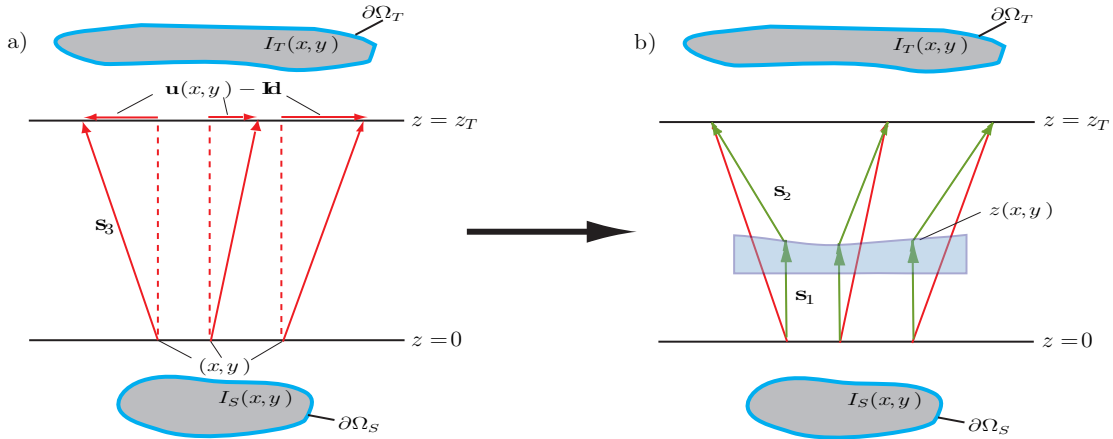


FIG. 1. a) For the given input intensity $I_S(x, y)$ and output intensity $I_T(x, y)$ the optimal ray mapping $\mathbf{u}(x, y)$ is calculated. The mapping defines a vector field \mathbf{s}_3 between the source plane $z = 0$ and the target plane $z = z_T$. $\partial\Omega_S$ and $\partial\Omega_T$ are the source and target intensity boundaries, respectively.

b) In the second process step the freeform surface $z(x, y)$ is constructed in a way that it is continuous and redirects the incoming collimated beam, described by the vector field \mathbf{s}_1 , according to the given optimal map. Because of energy conservation, the boundary of the freeform corresponds to the shape of the source intensity $\partial\Omega_S$.

plane.

We now know, that the source term of (8) has to vanish, but we are still left with the question, if we can find a way to fulfil condition (10). The main task is obviously to find a ray mapping for which relation (10) holds, which is nontrivial, since it couples the mapping with the unknown function $z(x, y)$.

But if we use the optimal mapping, it follows from its vanishing curl that $\nabla\mathbf{v} = 0$. If we use in addition to that, the small angle approximation

$$\mathbf{n} \cdot \mathbf{s}_2 \gg n_1 \cdot \mathbf{v} \cdot [(\mathbf{v}^\perp \cdot \nabla) \mathbf{v}^\perp] \quad (11)$$

between the surface normal $\mathbf{n}(x, y)$ and the outgoing ray $\mathbf{s}_2(x, y)$, we see that the condition (10) can be fulfilled approximately. Because of the fact that $\mathbf{n} \cdot \mathbf{s}_2$ is proportional to the source target distance z_T in contrast to the RHS, (11) can be interpreted as a far field approximation.

Hence for an optimal mapping and the small angle approximation, we get our final equation

$$\mathbf{v} \nabla z(x, y) = \nabla(\mathbf{v} \cdot z(x, y)) = 0, \quad \mathbf{v} = (\mathbf{u}(x, y) - \mathbf{Id})^\perp \quad (12)$$

which has to be solved to get the required freeform surface $z(x, y)$.

2. Boundary conditions

If we want to solve a linear advection equation like (12), we have to know the function $z(x, y)$ on the inflow part of the boundary, where the velocity field points into the integration area Ω_S [18]. Because of energy conservation, this area is defined as $\Omega_S := \{(x, y) \in \mathbb{R}_2 \mid I_S(x, y) \neq 0\}$

and therefore its inflow part by $\partial\Omega_{S-} := \{(x, y) \in \partial\Omega_S \mid \mathbf{v} \cdot \hat{\mathbf{r}} < 0\}$ with the outward boundary normal $\hat{\mathbf{r}}$. Together with this boundary condition equation (12) has at most one solution [18].

In our case the boundary conditions can be deduced in the following way. First, we have to realize, that for an incoming collimated beam the boundary of the freeform surface can only determine the tangential deflection of a ray refracted at the boundary. The normal deflection is determined by the inner parts of the surface $z(x, y)$. Therefore it makes sense to parameterize the boundary $\partial\Omega_S$ by a parameter s and define the local coordinate system at each point of the boundary by the vectors (see Fig. 2)

$$\mathbf{t} = \frac{d}{ds} \begin{pmatrix} x(s) \\ y(s) \\ 0 \end{pmatrix}, \quad \mathbf{r} = \frac{d}{ds} \begin{pmatrix} y(s) \\ -x(s) \\ 0 \end{pmatrix}, \quad \mathbf{e}_z = \begin{pmatrix} 0 \\ 0 \\ 1 \end{pmatrix}. \quad (13)$$

Since $z(s), s \in \partial\Omega_S$ only determines the tangential deflection, it is sufficient to consider the law of refraction (4) in the tangential plane spanned by $\hat{\mathbf{t}}(s)$ and \mathbf{e}_z . Hence, we can interpret the boundary value calculation as a two dimensional problem which allows us to derive a differential equation for the boundary values $z(s)$ by the two dimensional equivalent of equation (9) projected on the $\hat{\mathbf{t}}(s) - \mathbf{e}_z$ plane

$$\frac{\mathbf{n}}{(\mathbf{n})_z} \stackrel{!}{=} \begin{pmatrix} -\partial_l z(l) \\ 1 \end{pmatrix}, \quad l(s) := \int_0^s \sqrt{\left(\frac{dx}{dt}\right)^2 + \left(\frac{dy}{dt}\right)^2} dt, \quad (14)$$

where path length $l(s)$ was introduced for dimensional

reasons. From this we get:

$$\partial_s z(s) = -\frac{\mathbf{s}_2 \cdot \mathbf{t}}{(z_T - z(s)) - \frac{n_1}{n_2} \sqrt{(\mathbf{s}_2 \cdot \hat{\mathbf{t}})^2 + (z_T - z(s))^2}} \quad (15)$$

which reduces in the far field to

$$\partial_s z(s) \xrightarrow{z_T \rightarrow \infty} -\frac{\mathbf{s}_2 \cdot \mathbf{t}}{z_T \left(1 - \frac{n_1}{n_2}\right)} = \frac{v_x \partial_s y - v_y \partial_s x}{z_T \left(1 - \frac{n_1}{n_2}\right)}, \quad (16)$$

whereby the position of the surface in space compared to the target plane is fixed by integration constant. Since (12) itself can be interpreted as a far field approximation, as explained above, equation (16) seems more suitable for our purposes. It provides us with a simple way of calculating the boundary values. The only degree of freedom left is the integration constant. Equation (16) will build the basis of the numerical algorithm for solving equation (12) presented in the next section.

At the end of this section, we want to note that (12) and (16) can be derived analogously for freeform mirrors by replacing (4) by the law of reflection and keeping in mind that $z_T < z(x, y)$.

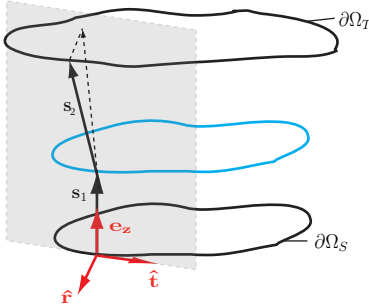


FIG. 2. The boundary $\partial\Omega_S$ is parameterized by s . At each point of the boundary the local coordinate system is spanned by the tangential vector $\hat{\mathbf{t}}$ and normal vector $\hat{\mathbf{r}}$ to the boundary as well as the unit vector \mathbf{e}_z . Since the boundary values $z(s)$ of the freeform surface only determine the tangential deflection of the rays hitting the boundary, the projection of the law of refraction (4) on the $\hat{\mathbf{t}}(s) - \mathbf{e}_z$ -plane can be used for the calculation of the boundary values.

III. NUMERICAL ALGORITHM

We could solve equation (12) by standard computational fluid dynamic approaches, like finite volume methods, which are appropriate for the numerical treatment of linear advection equations. Based on the nature of equation (16), a different approach is proposed in the following.

Considering (16), we recognize that the boundary values are calculated by the velocity field itself. This is in contrast to the usual fluid dynamical framework and allows

us to separate Ω_S into an arbitrary number of subareas $\Omega_{S,i}$ for each of which we can calculate the boundary values by (16). Therefore, the freeform surface can be calculated on each subarea $\Omega_{S,i}$ and the solution on Ω_S by their unification.

Hence, the most convenient way to get the solution of (12) seems to be a line-by-line integration of (16), which along the x - and y -direction is equivalent to equation (9) in a far field approximation. One possible way of integrating (16) is shown as an example in Fig. 3. Thus, only the integration constant of one integral has to be fixed from which the others follow automatically.

The proposed approach has the useful feature that we do not need to parametrize the boundary $\partial\Omega_S$, which allows the calculation of freeform surfaces with complex boundary shapes. The efficiency of the line-by-line integration approach is shown in the next chapter for two challenging design examples.

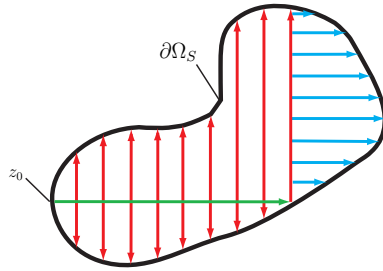


FIG. 3. The figure shows one possible way of solving the linear advection equation (12) by the simple integration of (16) along straight lines. First the value $z_0 = z(x_0, y_0)$ is fixed and used for the integration along the green line. The values of $z(x, y)$ on the green line serve as starting values for the line-by-line integration along the red lines in the orthogonal direction. Then the blue lines are integrated by using the values of $z(x, y)$ on the last red line.

IV. EXAMPLES

To show the efficiency of our algorithm, we want to apply it to two design examples. In the first one, we will calculate a freeform lens that maps a collimated beam of uniform intensity on the logo of the Institute of Applied Physics (IAP) in Jena with a resolution of 400 x 400 pixels (see Fig. 4). It shows strong intensity gradients between the letters and the background. To omit a division by zero within the implemented OMT algorithm [17] we have to use a background intensity $I > 0$ for the input and output intensities. For an appropriate speed of convergence the background intensity is set to 20 per cent of the maximum intensity. The second example, which shows smooth intensity variations and a lot of details, is the well-known picture of Lena with a resolution of 250 x 250 pixels (see Fig. 4).

Since the freeforms were calculated by integrating equa-

tion (16), the specific characteristics of both pictures do not have any influence on the speed of the lens construction step explained in section III, but they increase the mapping calculation time.

The pictures both have a square format. Hence, it is convenient to integrate first along the upper side of the square region and then line-by-line in the orthogonal direction with the starting values given by the first integration. Therefore we have to solve 401 and 251 integrals, respectively, which took in both cases less than one second in MATLAB on an Intel Core i3 at 2.4Ghz with 16GB RAM. This time has to be added up with the mapping calculation time, which strongly depends on the implemented method and the specific features of the picture. The integration constant on the upper left side of the integration area was chosen to be $z_0 = 1$. Values of $n_1 = 1.5$ and $n_2 = 1$ were used for the refractive indices, and the source-target distance was chosen to be $z_T = 5$. The input and output beam as well as the freeform lens had side length of one. Since every spatial value is normalized the results are scalable.

At this point we want to note that according to (16) the validity of the approximation (11) can simply be checked by scaling the numerical results with $1/z_T$, which of course has to be done for each intensity and configuration individually. For our examples the quality of the illumination patterns produced by the raytracing did not change significantly even for distances between the lens and the target plane smaller than the side length of the lens.

In both cases the calculated freeform lens was imported as a grid sag surface into ZEMAX to verify our results by a raytracing simulation. The imported lens data are interpolated by ZEMAX automatically. The results can be seen in Fig. 4.

V. CONCLUSION

We have presented an new effective numerical method for the single freeform surface design for the shaping of collimated beams. It is based on the fact that we could show that the design problem can be decoupled for a small angle approximation into two separate steps: the calculation of the optimal mapping and the construction of the freeform surface with a steady linear advection equation. On the basis of the finding of appropriate boundary conditions for the advection equation, we proposed a simple numerical algorithm for the lens construction by solving standard integrals. The generalization of our approach to double freeforms, point sources and near field calculations is currently under work.

APPENDIX A

We want to derive equation (8) from the law of refraction (4) and the integrability condition (5). Since the curl of the incident field $\hat{\mathbf{s}}_1$ vanishes, plugging (4) into (5) gives

$$\mathbf{n} \cdot \left(\nabla \times \frac{\mathbf{s}_2}{|\mathbf{s}_2|} \right) = \mathbf{n} \cdot \left(\frac{1}{|\mathbf{s}_2|} \nabla \times \mathbf{s}_2 - \mathbf{s}_2 \times \nabla \frac{1}{|\mathbf{s}_2|} \right) = 0 \quad (A1)$$

With

$$\nabla \frac{1}{|\mathbf{s}_2|} = -\frac{1}{2|\mathbf{s}_2|^3} \nabla (\mathbf{s}_2 \cdot \mathbf{s}_2) = -\frac{1}{|\mathbf{s}_2|^3} [\mathbf{s}_2 \times (\nabla \times \mathbf{s}_2) + (\mathbf{s}_2 \nabla) \mathbf{s}_2]$$

it follows

$$\mathbf{s}_2 \times \nabla \frac{1}{|\mathbf{s}_2|} = -\frac{1}{|\mathbf{s}_2|^3} \left\{ \underbrace{\mathbf{s}_2 \times [\mathbf{s}_2 \times (\nabla \times \mathbf{s}_2)]}_{= [\mathbf{s}_2 (\nabla \times \mathbf{s}_2)] \mathbf{s}_2 - |\mathbf{s}_2|^2 (\nabla \times \mathbf{s}_2)} + \mathbf{s}_2 \times [(\mathbf{s}_2 \nabla) \mathbf{s}_2] \right\} \quad (A2)$$

and we can write (A1) as

$$\mathbf{n} \cdot \{ [\mathbf{s}_2 (\nabla \times \mathbf{s}_2)] \mathbf{s}_2 + \mathbf{s}_2 \times [(\mathbf{s}_2 \nabla) \mathbf{s}_2] \} = 0. \quad (A3)$$

Inserting (4) and using $\hat{\mathbf{s}}_1 = (0, 0, 1)$ and $\hat{\mathbf{s}}_2 \cdot (\mathbf{s}_2 \times \dots) = 0$ leads to

$$(\mathbf{n} \cdot \mathbf{s}_2) \cdot [\mathbf{s}_2 (\nabla \times \mathbf{s}_2)] + n_1 \{ \mathbf{s}_2 \times [(\mathbf{s}_2 \nabla) \mathbf{s}_2] \}_z = 0 \quad (A4)$$

and with $\mathbf{s}_2 = \mathbf{s}_3 - \mathbf{s}_1$ it follows

$$\mathbf{s}_2 (\nabla \times \mathbf{s}_1) = n_1 \frac{\{ \mathbf{s}_2 \times [(\mathbf{s}_2 \nabla) \mathbf{s}_2] \}_z}{\mathbf{n} \cdot \mathbf{s}_2} + \mathbf{s}_2 (\nabla \times \mathbf{s}_3). \quad (A5)$$

Using the definition $\mathbf{v} = (-(\mathbf{s}_2)_y, (\mathbf{s}_2)_x)$ and (6) the terms in equation (A5) can be written as

$$\mathbf{s}_2 (\nabla \times \mathbf{s}_1) = \begin{pmatrix} -(\mathbf{s}_2)_y \\ (\mathbf{s}_2)_x \end{pmatrix} \cdot \begin{pmatrix} \partial_x z(x, y) \\ \partial_y z(x, y) \end{pmatrix} = \mathbf{v} \nabla z(x, y) \quad (A6)$$

and

$$\begin{aligned} \{ \mathbf{s}_2 \times [(\mathbf{s}_2 \cdot \nabla) \mathbf{s}_2] \}_z &= (\mathbf{s}_2)_x \cdot [(\mathbf{s}_2 \cdot \nabla) \mathbf{s}_2]_y - (\mathbf{s}_2)_y \cdot [(\mathbf{s}_2 \cdot \nabla) \mathbf{s}_2]_x \\ &= \begin{pmatrix} -(\mathbf{s}_2)_y \\ (\mathbf{s}_2)_x \end{pmatrix} \cdot \left[(\mathbf{s}_2 \cdot \nabla) \begin{pmatrix} (\mathbf{s}_2)_x \\ (\mathbf{s}_2)_y \end{pmatrix} \right] \\ &= \mathbf{v} \cdot [(\mathbf{v}^\perp \cdot \nabla) \mathbf{v}^\perp] \end{aligned} \quad (A7)$$

and

$$\begin{aligned} \mathbf{s}_2 (\nabla \times \mathbf{s}_3) &= (z_T - z(x, y)) \cdot [\partial_x (\mathbf{s}_2)_y - \partial_y (\mathbf{s}_2)_x] \\ &= -(z_T - z(x, y)) \nabla \mathbf{v}. \end{aligned} \quad (A8)$$

FUNDING INFORMATION

Federal Ministry of Education and Research Germany; project KoSimO (FKZ 031PT609X).

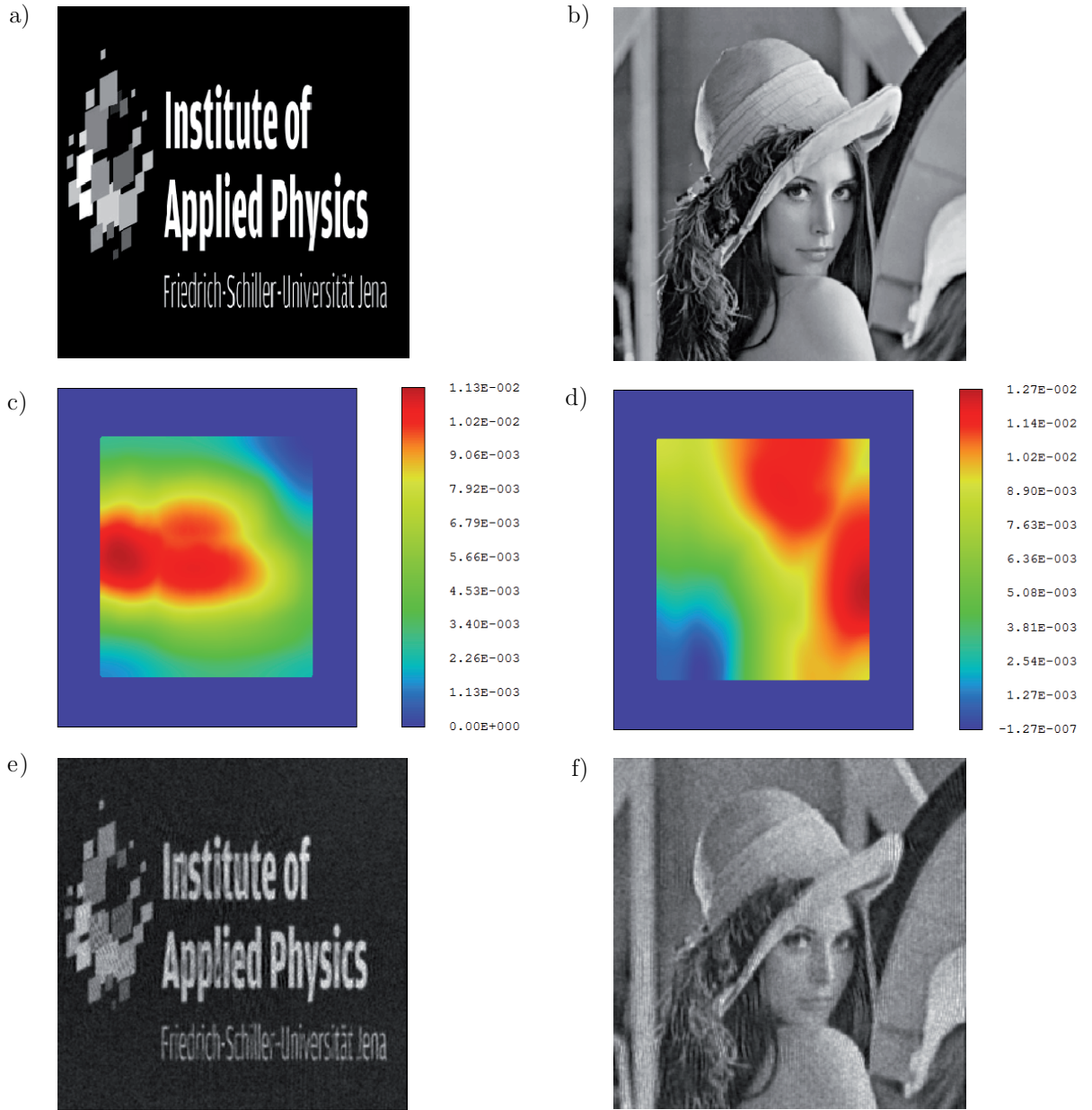


FIG. 4. a), b): given output intensities. In both cases, the incoming collimated beam was chosen to have a uniform intensity. c), d): false color maps of the calculated freeform lenses with side length of one. The integration constant of equation (16) at the upper left side was $z_0 = 1$ and the source-target distance $z_T = 5$. The imported numerical data was interpolated automatically by ZEMAX.

e), f): intensity pattern from a ZEMAX raytracing with 10^7 rays. The IAP logo shows some slight inhomogeneities, which are due to the slow convergence of the OMT algorithm [17] for pictures with numerous steep intensity gradients.

ACKNOWLEDGMENTS

The authors thank M. Esslinger, R. Hambach, S. Schmidt and M. Tessmer for valuable discussions, C. Liu and D. Lokanathan for the help with the ZEMAX implementation and D. Musick for the spelling and grammar check.

[1] H. Ries and J. Muschaweck, *J. Opt. Soc. Am. A* **19**, 590–595 (2002).

[2] R. Wu, L. Xu, P. Liu, Y. Zhang, Z. Zheng, H. Li, and X. Liu, *Opt. Lett.* **38**, 229–231 (2013).

[3] R. Wu, K. Li, P. Liu, Z. Zheng, H. Li, and X. Liu, *Appl. Opt.* **52**, 5272–5278 (2013).

[4] R. Wu, P. Liu, Y. Zhang, Z. Zheng, H. Li, and X. Liu, *Opt. Express* **21**, 20974–20989 (2013).

[5] Y. Zhang, R. Wu, P. Liu, Z. Zheng, H. Li, and X. Liu, *Opt. Comm.* **331**, 297–305 (2014).

[6] C.R. Prins, J.H.M. ten Thije Boonkkamp, J. Van Roosmalen, W.L. IJzerman, and T.W. Tukker, *SIAM J. Sci. Comput.* **36**, B640–B660 (2014).

[7] V.I. Oliker, in *Trends in Nonlinear Analysis*, M. Kirklionis, S. Kromker, R. Rannacher, and F. Tomi, eds. (Springer-Verlag, 2003), pp. 193–222.

[8] F.R. Fournier, W.J. Cassarly, and J.P. Rolland, *Opt. Express* **18**, 5295–5304 (2010).

[9] C. Canavesi, W.J. Cassarly, and J.P. Rolland, *Opt. Lett.* **38**, 5012–5015 (2013).

[10] D. Michaelis, D. Schreiber, and A. Bruer, *Opt. Lett.* **36**, 918–920 (2011).

[11] A. Buerle, A. Bruneton, P. Loosen, and R. Wester, *Opt. Express* **20**, 14477–14485 (2012).

[12] A. Bruneton, A. Buerle, P. Loosen, and R. Wester, *Opt. Express* **21**, 10563–10571 (2013).

[13] Z. Feng, L. Huang, G. Jin, and M. Gong, *Opt. Express* **21**, 14728–14735 (2013).

[14] Z. Feng, L. Huang, G. Jin, and M. Gong, *Opt. Express* **21**, 28693–28701 (2013).

[15] J.-D. Benamou, Y. Brenier, and K. Guittet, *Int. J. Numer. Meth. Fluids* **40**, 21–30 (2002).

[16] S. Haker, L. Zhu, A. Tannenbaum, and S. Angenent, *Int. J. Comp. Vis.* **60**, 225–240 (2004).

[17] M.M. Sulman, J.F. Williams, and R.D. Russel, *Appl. Numer. Math.* **61**, 298–307 (2011).

[18] D. Kuzmin, *A Guide to Numerical Methods for Transport Equations* (University Erlangen-Nuremberg, 2010).